Comparative Evaluation of Optical–SAR Feature-Level Fusion Using Sentinel-1 VH and VV Polarizations for Land Use/Land Cover Classification in Semi-Arid Environments

Abed Touma Jasim[1], Sadra Karimzadeh[2]✉, Abolfazl Ghanbari[3], Muntadher Aidi Shareef[4]

1. Department of Surveying Technical Engineering / Faculty Technical Engineering / Northern Technical University, Kirkuk 36001, Iraq. E-mail: abedtuama@ntu.edu.iq
2. Corresponding author, Department of Remote Sensing and GIS, Faculty of Planning and Environmental Sciences, University of Tabriz, Tabriz, Iran. E-mail: sadra.karimzadeh@gmail.com
3. Department of Remote Sensing and GIS, Faculty of Planning and Environmental Sciences, University of Tabriz, Tabriz, Iran. E-mail: a_ghanbari@tabrizu.ac.ir
4. Department of Surveying Technical Engineering / Faculty Technical Engineering / Northern Technical University, Kirkuk 36001, Iraq. E-mail: muntadher.a.shareef@ntu.edu.iq

Article Info

Article type:
Research Article

Article history:
Received: 7 June 2026
Revised: 12 July 2026
Accepted: 18 August 2026
Published: 22 August 2026

Keywords:
Sentinel 1 SAR,
image fusion,
LULC,
VH polarization,
VV polarization,
Desertification,
agricultural degradation,
urban expansion,
SVM.

ABSTRACT

Monitoring land-use/land-cover (LULC) dynamics is essential for understanding environmental change and supporting sustainable land management in semi-arid regions. This study evaluates feature-level Optical–SAR fusion by integrating Landsat multispectral imagery with Sentinel-1 VV and VH backscatter data for LULC classification and change detection in Kirkuk City, Iraq, between 2015 and 2024. Five land-cover classes—desert, barren land, agriculture, water, and built-up areas—were classified using a Support Vector Machine (SVM) classifier and assessed with overall accuracy (OA), Kappa coefficient, producer's and user's accuracies, and confusion matrices. The Landsat + Sentinel-1 VV fusion dataset achieved the highest classification accuracy in 2015 (OA = 96.51%, Kappa = 0.954). However, by 2024, increasing landscape complexity reduced classification performance for both fusion datasets. Change detection revealed substantial environmental transformations, with agricultural degradation as the dominant transition. Agricultural land decreased by 45.40% and 30.15%, primarily converting to barren land in the VH and VV fusion datasets, respectively. Additional transitions from agriculture and barren land to desert indicate accelerating desertification, while built-up areas showed persistent expansion, largely at the expense of agricultural land. Confusion matrix analysis also revealed increasing spectral similarity between barren land and desert, suggesting the emergence of transitional degradation zones. Overall, the findings identify agricultural degradation, desertification, and urban expansion as the principal environmental processes shaping the study area and demonstrate the value of Sentinel-1 VV and VH data integrated with Landsat imagery for operational LULC monitoring in semi-arid environments.

Cite this article: Touma Jasim, A., Karimzadeh, S., Ghanbari, A. & Aidi Shareef, M. (2026). Comparative Evaluation of Optical–SAR Feature-Level Fusion Using Sentinel-1 VH and VV Polarizations for Land Use/Land Cover Classification in Semi-Arid Environments. *Journal of Remote Sensing and GIS Applications in Environmental Sciences*, 6 (19), 75-96. http//doi.org/10.22034/rsgi.2026.72860.1164

© The Author(s).
Publisher: University of Tabriz.
DOI: http//doi.org/10.22034/rsgi.2026.72860.1164

Introduction

LULC dynamics are among the most critical indicators of change, especially in semi-arid regions where ecosystems are highly vulnerable to climatic variability, human activity, and resource exploitation. Long-term observation of LULC changes is an important means of detecting environmental degradation, urbanization, sustainable agricultural development, and desertification processes, which have far-reaching impacts on ecosystem services and regional growth [1,2].

Land degradation is a pressing and significant global issue, and semi-arid environments are particularly susceptible to this threat: the challenges of nationwide water scarcity and repeated droughts, as well as additional human-induced activities such as soil salinization, can result in highly productive soils transitioning into useless or desert surfaces [3,4]. The increased population growth and urbanization in Iraq and the Middle East have placed additional stress on agricultural resources, leading to significant changes in landscape structure and ecological stability [5]. Hence, real-time monitoring of LULC changes is a necessity for sustainable land management and environmental planning.

Satellite remote sensing technologies provide a large-scale, long-term environmental monitoring platform. Optical satellite sensors (e.g., Landsat) provide spectral information for characterizing vegetation, water bodies, urban areas, and bare surfaces [1,6]. But optical imagery can also be affected by atmospheric conditions, illumination variations, and seasonality. In stark contrast, Synthetic Aperture Radar (SAR) systems operate day and night in any weather [7], providing complementary information on surface roughness, soil moisture content, and vegetation structure. As a result, fusing optical and SAR data has many advantages for enhancing the accuracy of LULC classification and environmental monitoring [8].

Sentinel-1 is a dual-polarized C-band SAR mission with freely available data, providing vertical transmit–vertical receive (VV) and vertical transmit–horizontal receive (VH) radar observations [9] Therefore, it is one of the most interesting current spaceborne missions in terms of image accessibility. VV and VH polarization responses vary with land-cover characteristics, vegetation structure, and surface conditions, and these have been extensively studied in the past, which helps in carrying out environmental applications or change-detection studies [10,11]. VH observations are often more sensitive to vegetation volume scattering than those at VV polarization, leading to stronger signals from urban and bare surfaces [2,12]. This highlights the importance of assessing performance between polarization-based fusion strategies for land-cover discrimination and environmental change assessment [12].

With the development of data fusion techniques, it has gained a crucial role in modern remote-sensed data processing, as it combines sensors with different spatial resolutions [13,14], offering complementary information for higher classification performance and better thematic mapping accuracy [15]. Some studies noted that joint optical and SAR observations would considerably help to discriminate spectrally similar land-cover classes, which was especially valid for heterogeneous or environmentally stressed landscapes [16,17]. However, uncertainty in classification remains elevated in semi-arid regions where transitional surfaces among agricultural, barren, and desert environments exhibit similar spectra and radar backscatter responses [18].

Kirkuk City, situated in northern Iraq, would be a representative case study for investigating these challenges due to rapid urbanization, high agricultural pressures, limited water resources, and increasing environmental pressures [19]. This region has undergone significant landscape changes over the past 10 years, providing an important testbed for assessing the performance of integrated optical-SAR methods in detecting and quantifying environmental change [20]. Disentangling these complexities is vital for facilitating sustainable land-use planning and stemming future land degradation.

Research Gap

Despite the increasing use of optical and SAR remote sensing data for LULC mapping, few studies have systematically evaluated the contribution of Sentinel-1 VH and VV polarizations within a feature-level Optical–SAR fusion framework in semi-arid environments. Furthermore, previous studies conducted in Iraq and the Kirkuk region have primarily relied on optical imagery or single-sensor approaches, with limited attention to polarization-specific fusion strategies and their influence on classification accuracy and long-term LULC change detection. Therefore, a comprehensive comparison of Landsat–Sentinel-1 VV and Landsat–Sentinel-1 VH feature-level fusion datasets remains lacking. This study addresses this gap by evaluating both fusion scenarios using SVM classification and assessing their effectiveness for LULC mapping and environmental change detection between 2015 and 2024.

Thus, the primary aim of this study is to evaluate the performance of feature-level Optical–SAR fusion datasets generated by integrating Landsat multispectral imagery with Sentinel-1 VV and VH SAR backscatter data for LULC classification and change detection in a semi-arid environment in Kirkuk City, Iraq. To clarify more the objectives of this study are to: (1) assess classification performance of fusion datasets using support vector machine (SVM) classification in VH and VV bands; (2) better understand class-level accuracies and classify uncertainties; (3) identify spatially and temporally land use/land cover changes between 2015 and 2024; and (4) examine certain dominant environmental processes affecting the study area such as agricultural degradation, desertification, urban expansion. The results enhance understanding of environmental change processes in semi-arid regions and demonstrate the benefits of integrated optical–SAR remote sensing for sustainable land management and long-term environmental monitoring.

Research Questions

Based on the identified research gap, this study addresses the following research questions:

RQ1: Does feature-level Optical–SAR fusion using Landsat multispectral imagery with Sentinel-1 VV polarization provide higher LULC classification accuracy than fusion using Sentinel-1 VH polarization?

RQ2: What are the dominant land-use/land-cover (LULC) changes that occurred in Kirkuk City between 2015 and 2024?

RQ3: How effective is the proposed feature-level Optical–SAR fusion approach combined with SVM classification for long-term environmental change detection in a semi-arid environment?

Study area

Located about 250 km north of Baghdad, Kirkuk City is considered one of the most significant socio-economic and cultural hubs in northern Iraq. At the administrative level, Kirkuk Governorate includes four major districts: Kirkuk District, Hawija District, Daquq District, and Dibis (Figure 1). Its geographic position in Iraq and heterogeneous population give it significant economic and political power to influence the rest of the country. The area of study selected for this work is central Kirkuk City, an area with distinctive, rapid-scale growth and heterogeneous change in land-use/land-cover [21].

Kirkuk Sirwan's climate is semi-arid, featuring highly seasonal temperature variation and long hot summers. Favorable summer temperatures between 40 and 50 °C and unfavorable winter temperatures (−5 to 5 °C) influence ecological features, land-use concepts, agricultural systems, and settlement structures in the region. including the existence of arable agricultural patterns, irrigation systems, and super-diverse terrain types (plains with symbol; lowlands locally known as "Achon" [Kurdish]; highlands), adding to the diversity of environmental conditions in the study area17.

Study Area and Kirkuk Governorate (Fig- 1). The map was built on a traditional cartographic framework of a scale bar, a north arrow, a coordinate grid, and an inset map showing the regional location of the study area. To facilitate spatial coherence for geospatial analysis, all spatial data layers

used in the current study were projected to the WGS 1984/UTM Zone 38N coordinate reference system [23].

The study area, which is less than 100 km², is located in the middle of Kirkuk City at the coordinates (35.10° N, 35. 20° E and 44.25° N of the Great Rift Valley, Africa (Figure 1). Elevation ranges from around 341—346 m above mean sea level. The Climate Here is Semi-Arid, With Hot, Dry Summers and Mild, Wet Winters. The general land-use/land-cover classes are 1. Agricultural Land,2. Barren Land (Desert),3. Built-Up Areas and water bodies. Kirkuk city center was selected as the potential region of interest for this study due to rapid urban sprawl, agricultural degradation, and increasing desertification in the past ten years, making it an ideal site to evaluate feature-level Optical–SAR fusion for LULC classification and long-term environmental change detection.

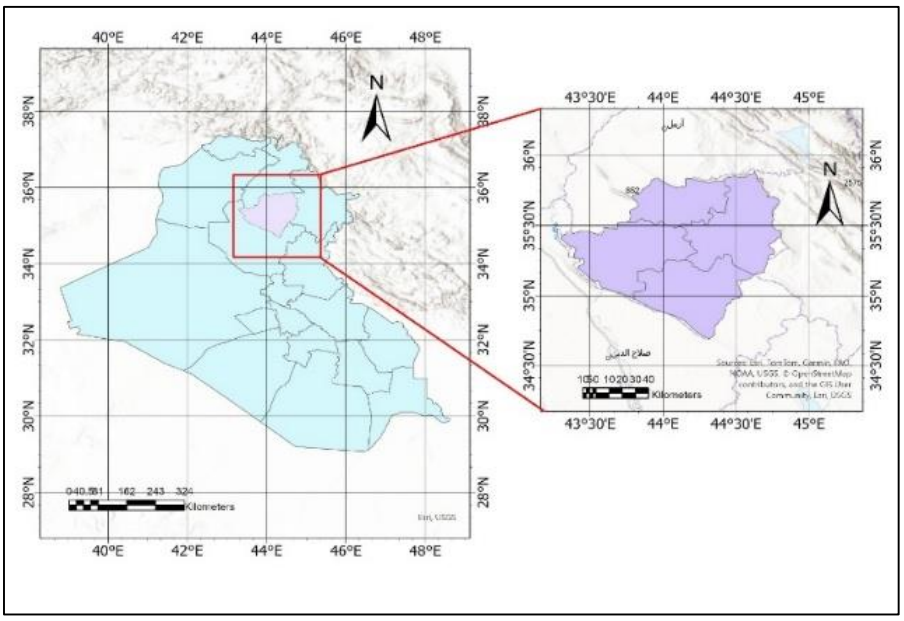


Figure 1. Location of the Study Area in Central Kirkuk City, Kirkuk Governorate, Iraq.

Materials and Method

Figure 1 presents a schematic overview of the study's methodological framework, which employs a multi-satellite, remote-sensing data-based LULC classification and change-detection approach. It begins with collecting satellite imagery from different sources (satellite optical data and SAR datasets), running preprocessing, which prepares (or validates through checking the input data so as to be complete + accurate). In the preprocessing step, it also provides independent processing chains for both radar and optical imagery; starting tasks include radiometric and geometric correction, noise reduction, image clipping, and calibration. Then, features from both spectra and radar sensors are extracted from the two preprocessed datasets and integrated using a data fusion approach to improve classification performance. Then, to perform supervised classification, we select training and test samples. An image classification, followed by thematic land use and land cover (LULC) maps that explicitly illustrate the spatial distribution of the dominant land cover type across different locations within the study area, is then used to characterise LULC. After classification, we apply post-classification refinement methods, such as major/minor analysis and sieve-measure class, to reduce noise introduced during classification and obtain a clean land cover map. To evaluate the accuracy of these maps, their constitutive elements (classification) are assessed using conventional classification assessment methods, since the outcome maps need to be valid. In the end, change detection analysis is adapted to investigate spatial and temporal changes in land use/cover patterns and to produce outputs for mapping/modelling/interpreting environmental changes at the studied sites.

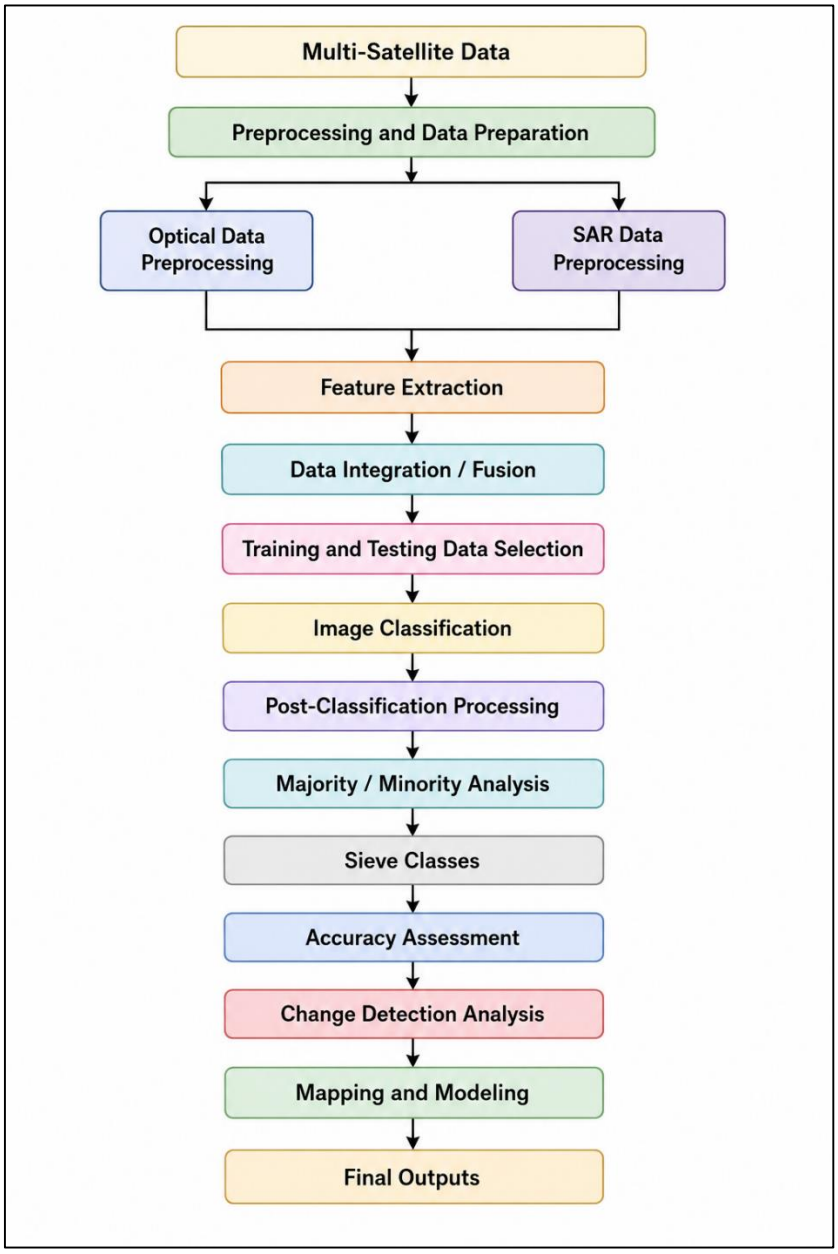


Figure 2. General Methodology.

Data used

This study used multi-source satellite datasets that capture both optical and Synthetic Aperture Radar (SAR) imagery to examine LULC changes in a selected area, which is the center of Kirkuk City, Iraq. Table 1: Data characteristics of the satellite data used in this study. Landsat-8 OLI/TIRS imagery (from 23 July 2015) and Landsat-9 OLI/TIRS imagery (from 11 October 2024), with a spatial resolution of 30 m, were also used as optical datasets. Moreover, Sentinel-1 IW GRDH SAR imagery in dual polarizations (VH and VV) with a spatial resolution of 10 m was used for the years of interest (i.e., the satellite pass date). Sentinel-1 Interferometric Wide Swath (IW) Ground Range Detected High Resolution (GRDH) products were used in this study. Dual-polarization (VV and VH) C-band SAR imagery with a spatial resolution of 10 m was selected for its ability to provide reliable observations under all weather conditions and its sensitivity to surface roughness, soil moisture, and vegetation structure, making it suitable for Optical–SAR feature-level fusion and LULC classification.

The optical satellite imagery was downloaded from USGS Earth Explorer, and the SAR dataset was acquired through Copernicus Data Space Browser. The images were chosen based on image quality, acquisition season, and minimum cloud cover to ensure consistent and reliable analysis.

Ancillary datasets were added to inform the classification and validation processes, including relevant administrative boundary shapefiles, high-resolution RGB satellite imagery, and field-based observations. The additional datasets were used to inform classes and to validate the accuracy of the generated classification maps.

Table 1. image data used in this study

Data Type	Sensor	Product Type	Polarization	Acquisition Date	Spatial Resolution
SAR	Sentinel-1 IW GRDH	GRDH	VV, VH	25 Jul 2015	10 m
SAR	Sentinel-1 IW GRDH	GRDH	VV, VH	17 Oct 2024	10 m

Data preprocessing

Optical data preprocessing is the first step in processing remote sensing images, as it greatly enhances the stability and accuracy of subsequent classification and change detection [27]. Several preprocessing steps were performed on Landsat-8 and Landsat-9 images to produce suitable data for LULC classification in this study. They involved layer stacking, radiometric correction, mosaicking, and clipping images [24].

You can start by stacking multiple spectral bands into a single multispectral dataset. The integration of different spectral bands into a single descriptor is required, as each band contains distinct information about the physical and chemical properties of surface materials, thereby improving discrimination between land-cover features [25]. The comparison provided better spectral separability among urban areas, vegetation, bare soil, and water bodies in the study area.

Then, a radiometric correction process was performed to remove the effects of atmospheric disturbances, sensor- and illumination-related distortions. This improved the consistency of radiometry in imagery and made pixel values more representative of surface reflectance characteristics, thereby enhancing classification reliability [26].

After the correction processes, the satellite images were mosaicked in ENVI 5.6 to produce seamless and contiguous image coverage of the entire study area. The mosaicking can then combine multiple but geo-rectified scenes. Lastly, the imagery was clipped to the study area boundary located in the center of Kirkuk City. This unique preprocessing workflow established spatial consistency and further enhanced the functional relevance of the optical datasets for feature extraction, classification, and land-use/land-cover change analysis, as shown in Figure 2.

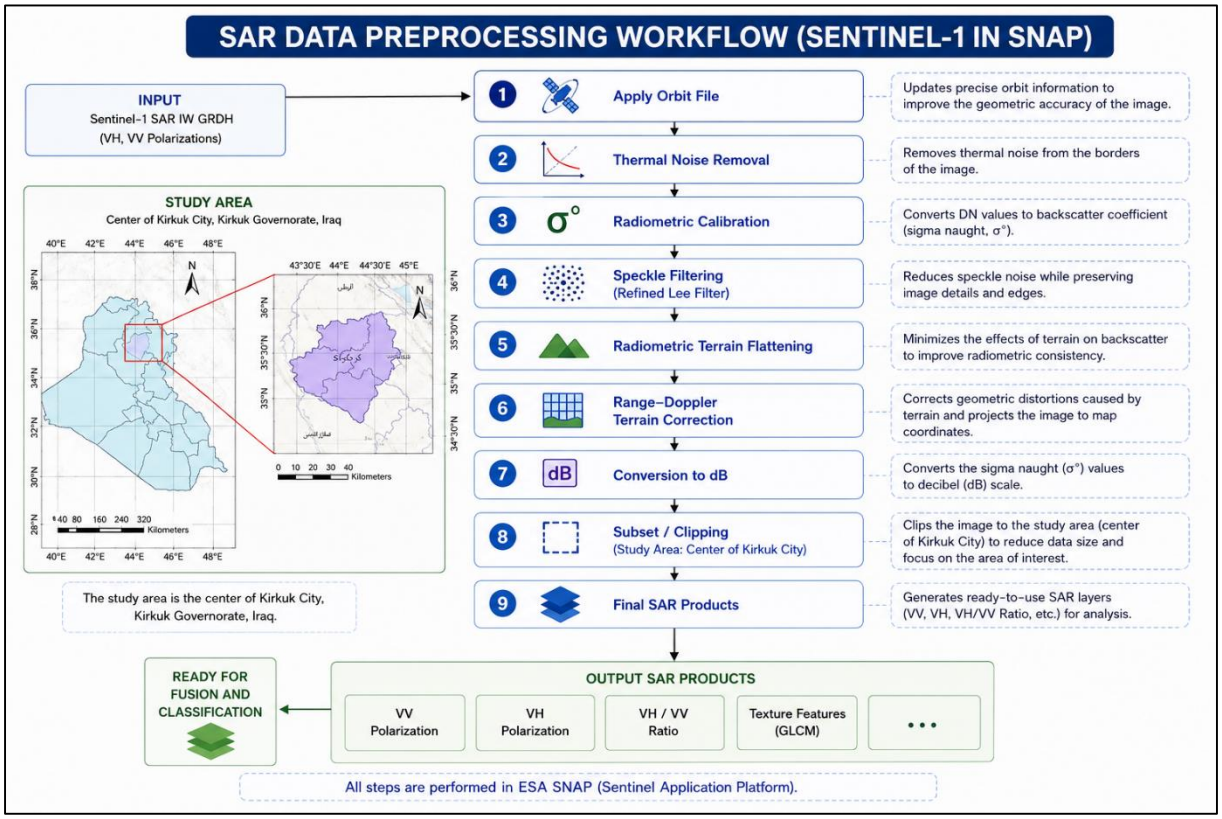


Figure 3. General methodology of SAR data preprocessing.

Figure 3. The general methodology for SAR data preprocessing was conceptually designed by the authors with support from AI-generated images and accurately reflects the preprocessing workflow implemented in ESA SNAP.

In the present case, the diagram in Figure 3 illustrates how to apply the preprocessing phase to Sentinel-1 SAR data, with the aim of performing land-use/land-cover classification at the core of Kirkuk City / Iraq, within the ESA SNAP environment. For this purpose, we use the first phase of the Magic Toolbox Preprocessing, which concerns dual-polarized (VV and VH) Sentinel-1 IW GRDH imagery. 1. Apply the orbit file - This geo-corrects the geometric quality of SAR imagery using accurate orbital data. Thermal Noise Removal is designed to mitigate border noise and radiometric distortions. Radiometric Calibration follows and converts the digital number (DN) values to σ° backscatter coefficients, which have physical meaning. The Refined Lee speckle filter is a non-linear post-processing technique that filters out speckle noise while retaining features and edges in the image. The next step involves applying Radiometric Terrain Flattening (RTF) to minimize terrain-induced radiometric variations and make the backscatter response more homogeneous across the entire study area. After that, we perform range-doppler terrain correction to remove geometric distortions and geo-reference the corrected image. The SAR backscatter values obtained from calibration are converted into dB and used for interpretation/classification. Afterward, we cropped the other eight processed images to the study area (the center section of Kirkuk City) to reduce data volume and focus the analysis on the area of interest. Finally, the preprocessing workflow provides functional SAR datasets, including VV- and VH-polarized layers and VH/VV ratio products, for input to land-use/land-cover classification and change-detection analyses.

Feature-Level Data Fusion

Feature-level fusion was adopted in this study using a band-stacking strategy. After preprocessing, the multispectral Landsat bands were concatenated with the Sentinel-1 SAR backscatter layer (either VV or VH polarization) to construct a unified multi-band feature dataset. Two independent fusion datasets

were generated: (i) Landsat + Sentinel-1 VV and (ii) Landsat + Sentinel-1 VH. Each fused dataset was then used separately as the input to the Support Vector Machine (SVM) classifier to evaluate the contribution of each SAR polarization to land-use/land-cover classification performance. This feature-level fusion preserves the complementary spectral information from optical imagery, along with the structural and moisture-sensitive information from SAR data, while avoiding the information loss associated with decision-level fusion. The fused feature vector can be expressed as a

$$F = [B_1, B_2, \dots\dots, B_{n,}S] \quad (1)$$

B_1= Landsat spectral bands.

S= Sentinel-1 VV or VH backscatter layer.

F = fused feature vecto.

Figure 4. illustrates the architecture of the feature-level Optical–SAR fusion process implemented in this study. After independent preprocessing, the Landsat multispectral bands and Sentinel-1 SAR backscatter layer (VV or VH) were integrated using a band-stacking approach to produce the fused feature vector used for SVM classification.

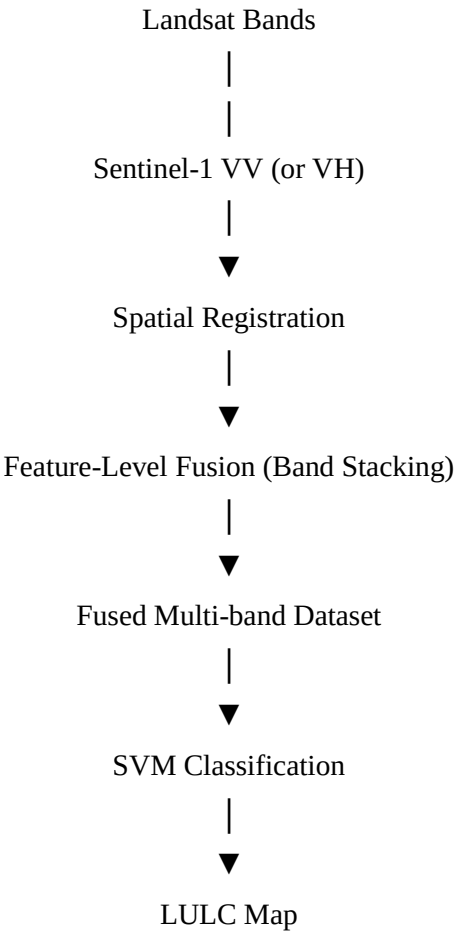


Figure 4. Feature-Level Optical–SAR Fusion Workflow Adopted In This Study.

Support vector machine

In recent literature, support vector machines (SVMs) can be used to reproduce the final result. It has been widely used in remote sensing image classification, as its experience can further reduce errors, and the shallow, sharp edge area geometric characteristic would be described [27]. SVM is a supervised classification algorithm based on statistical learning theory, which provides good

classification results in complex and noisy data [28]. The support vector machine is also employed for both linear and nonlinear classification. On the other hand, this method relies on a training method to classify [29].

SVM as the separable case

In order to explain this case strictly, suppose there are two classes separated linearly. Given a training set of instance-label pairs$\{x_i, y_i\}, i = 1, \ldots, n, y_i \in \{1, -1\}, x_i \in R^d$, where x_iHe observed a multispectral feature and y_i (either +1 or -1) denotes the information class label for training. The goal of a support vector classifier is to find a hyperplane (in infinite-dimensional space) that allows to separate two classes, and the distance from the hyperplane to the nearest training pixel in each class is maximum. The hyperplane can be represented as

$$w^T x + b = 0 \quad (2)$$

Where x is a point on the hyperplane, w is the normal to the hyperplane (i.e., the transpose of the weight vector), and b is the bias, which determines their location relative to the origin. Further, $|b|/\|w\|$ represent the perpendicular distance from the hyperplane to the origin $\|w\|$ is the Euclidean norm of w [30].

SVM classification and parameter tuning

In this study, LULC classification was performed using an SVM (Support Vector Machine) with a Radial Basis Function (RBF) kernel. This was explained by the fact that spectral mixing and similarity among LULC classes in multispectral remote sensing data often render them nonlinearly separable, and that RBFs can represent complex decision boundaries. The hyperparameters C and γ (gamma) were optimised using grid search with k-fold cross-validation (k = 5) on the training subset. The searching ranges were $C \in [0.1, 1000]$ and $\gamma \in [1\times10^{-4}, 1]$. The reference samples were split into 70% for training and 30% for independent validation (both training and validation samples were selected using stratified random sampling to ensure all LULC categories were sufficiently represented in each subset). Therefore, all hyperparameter settings were determined using training data only, and the validation set was kept completely independent for accuracy evaluation. But to facilitate direct comparison across years, all LULC maps were produced with a uniform legend and class order and printed at publication quality [30].

Change detection process

The major benefit of change detection is that information about land-cover change transactions can be produced accurately and free from atmospheric influences [31]. For this, a post-classification strategy for Land Use and Land Cover (LULC) change detection was employed. This approach compares pixels in an image from two dissimilar times to detect significant changes at pixel resolution [32]. The basis of this algorithm is to compute the change in cover between a reference thematic image and another classified image (to slightly paraphrase, an image need not be entirely arbitrary). Change detection includes a variety of methods to identify and characterize differences between data taken at different times. A post-classification comparison approach based on a transition matrix was adopted to quantify LULC changes between 2015 and 2024. The classified maps from the two dates were cross-tabulated to generate a transition matrix that records the number of pixels changing from each source land-cover class to each target class. This matrix-based approach is appropriate for categorical LULC maps and enables detailed analysis of class-to-class transitions while minimizing the influence of radiometric differences between acquisition dates.

$$P_{ij} = \frac{N_{ij}}{N_i} \text{ x } 100 \quad (3)$$

Where:

whereP_{ij} is the percentage of pixels that changed from land-cover class iii to class ij N_{ij} is the number of pixels that changed from class i; to class ij and $N_i$is the total number of pixels belonging to class iii in the reference year (2015).

The transition matrix was further used to calculate the percentage of each land-cover transition and to identify the dominant environmental processes, including agricultural degradation, desertification, and urban expansion. The resulting transition statistics were subsequently interpreted together with the classification accuracy assessment and spatial change-detection maps to provide a comprehensive evaluation of LULC dynamics within the study area.[33].

Results and Discussion

Classification Performance Assessment for 2015 and 2024

The performance of the Sentinel-1 VH and VV fusion classifications was evaluated using Overall Accuracy (OA) and the Kappa coefficient. Results showed significant contrasts between polarization modes and years, echoing differences in land-cover separability and environmental conditions.

Table 2. Overall Classification Accuracy Statistics for Sentinel-1 VH and VV Fusion Datasets in 2015 and 2024

Year	Fusion Dataset	Overall Accuracy (%)	Kappa Coefficient
2015	VH Fusion	84.93	0.800
2015	VV Fusion	96.51	0.954
2024	VH Fusion	80.31	0.734
2024	VV Fusion	78.94	0.715

The performance of the Sentinel-1 VH and VV fusion dataset for 2015 and 2024 is shown in Table 2. The results show that the 2015 VV fusion dataset has the highest OA (96.51%) and a Kappa of 0.954 between the classified map and the reference data, indicating good agreement. In contrast, the VA fusion dataset achieved an OA of 84.93% and a Kappa of 0.800 in the same year. In 2024, both polarization modes had lower accuracies because the OA values reduced to 80.31% for VH and 78.94% in VV classes. Likewise, the Kappa coefficients both dropped from 0.734 to 0.715. The decrease in classification performance is associated with more complex land cover and a progressive similarity between classes over time. Environmental degradation, loss of vegetation, and surface transitions between barren land and desert probably decreased class separability, thereby increasing classification uncertainty in the 2024 datasets.

Class-Level Classification Accuracy Analysis

To better understand class discrimination performance, Producer's Accuracy was analyzed for each land-cover category.

Table 3. Producer's Accuracy (%) of Land-Cover Classes for Sentinel-1 VH and VV Fusion Datasets in 2015 and 2024

Land-Cover Class	VH 2015	VV 2015	VH 2024	VV 2024
Barren Land	59.65	100.00	74.40	74.90
Desert	98.72	98.86	30.16	19.59
Agriculture	54.02	95.94	98.18	98.55
Water	100.00	100.00	100.00	100.00
Built-up Area	94.96	92.83	98.47	98.97

Table 3 presents the Producer's Accuracy (PA) for the land-cover classes derived from the Sentinel-1 VH and VV fusion datasets in 2015 and 2024. On the other hand, water was classified with perfect accuracy (100%), which indicates that SAR data is an excellent tool for detecting water bodies. Built-up areas had similarly high accuracies (>92%) due to the unique double-bounce scattering characteristic of urban features. Land-use improvement to >98% in both polarization modes for agricultural land by 2024. By contrast, the desert class showed a drastic decrease from> 99% in 2015 to only 30.16% (VH) and 19.59% (VV) in 2024, suggesting intense confusion with barren land. Consensually, the accuracy for barren land was also moderate, ranging from 59.65% to 74.90%. These results indicate an approaching similarity between barren and desert surfaces, consistent with continued land degradation and desertification, as the detailed study area shows.

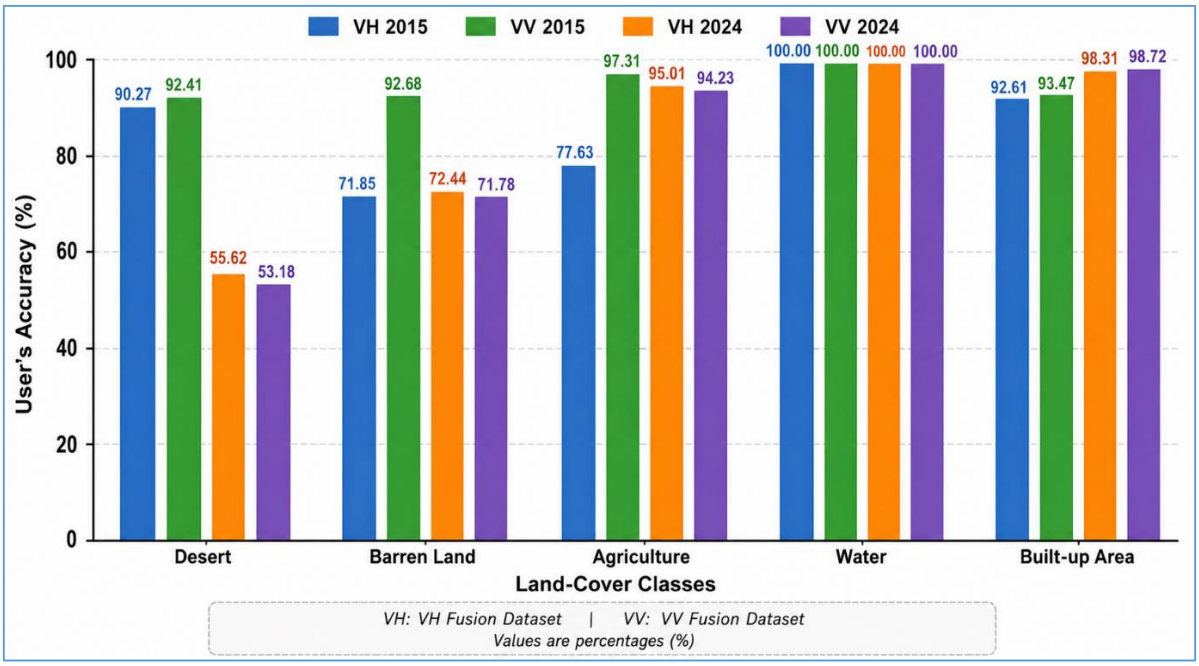


Figure 4. User's Accuracy Comparison of Individual Land-Cover Classes for 2015 and 2024.

The User's Accuracy (UA) for individual land-cover classes, based on the Sentinel-1 VH and VV fusion datasets in 2015 and 2024, is shown in Figure 4. Water showed the best classification reliability across datasets with almost perfect accuracy (100%). Urban features were also associated with high Kappa values (>92%); this is likely due to unique radar scattering characteristics between urban and non-urban areas. Agricultural Land performed relatively well in 2024, achieving around 95% accuracy. On the contrary, the desert class had a notable drop from above 90% in 2015 to 54–56% in 2024 due to huge confusion with barren land. Likewise, the accuracy of barren land decreased in 2024 compared to the VV-2015 level. Proceeding from this, the merger of barren and desert surfaces, based on evidence of degradation and advancing desertification, is increasingly evident. In general, the results show that, in 2024, the consistent reliability of water and built-up classes was lower than that of desert and barren land.

Classification Error Analysis

A confusion matrix analysis of the 2024 datasets indicated that the greatest classification uncertainty occurred between the desert and barren land categories. As shown in Table 4, 69.84% of desert reference samples were incorrectly classified as barren land in the VH dataset, and this proportion increased to 80.41% in the VV dataset. In contrast, particles of barren land were misclassified as desert with 25.60% and 25.10% in the VH and VV datasets, respectively. Most importantly, this mutual confusion suggests considerable overlap in the radar backscatter properties of the two classes. This type of behavior is often seen in land degradation, where bare surfaces increasingly exhibit the physical properties of desert regions due to the loss of vegetation cover, increased soil exposure, and

reduced moisture content. This suggests that the confusion being observed here is not just a classification limit but also a sign of ongoing environmental change. Yet, the increasing similarity between duneless and desert lands indicates that transitional degradation zones are developing and provides further evidence for the desertification types identified through change-detection analysis.

Table 4. Major Sources of Classification Confusion in the 2024 Datasets

Stable Transition	VH (%)	VV (%)
Desert → Desert	0.59	0.64
Barren Land → Barren Land	8.76	25.43
Agriculture → Agriculture	4.15	3.52
Water → Water	0.37	0.38
Built-up Area → Built-up Area	11.05	11.13
Total Stable Area	24.92	41.11

Furthermore, confusion matrix analysis indicated that the desert and barren land classes had the greatest classification uncertainty in the 2024 datasets. As detailed in Table 5, desert reference samples in the VH dataset were misclassified as barren land in 69.84% of total samples, and in 80.41% of total samples in the VV dataset. In contrast, 25.60% and 25.10% of the barren-land samples were misclassified as desert in the VH and VV datasets, respectively. This mutual confusion suggests a significant overlap between the two classes in radar backscatter features. This is a typical pattern of land degradation, in which the formerly barren surface acquires the physical characteristics of desert environments because plant cover, nutrients, and moisture are lost from the soil. Hence, the azimuthal confusion is not only a limitation of classification. Table 4 shows that the proportion of stable land-cover classes identified by the VV fusion dataset (41.11%) was much higher than that of the VH fusion dataset (24.92%), suggesting stronger temporal stability and better temporal robustness in detecting classification variability using VV data. In the VV dataset, barren land was by far the most stable class, remaining unchanged for 25.43% of the study area over time, whereas it was only 8.76% stable in the VH dataset. Built-up areas also exhibited high persistence, covering 11.05% and 11.13% of the total area in the VH and VV datasets, respectively, reflecting stable land use over the long term [40]. On the contrary, agricultural land had an overall low persistence of 6.67% (VH) and 5.13% (VV), confirming significant land-cover change over time. The combination of low areal stability for agriculture and an equally high persistence for barren and urban land indicates that agricultural lands played the most dynamic role in landscape change between 1988 and 2006. These results are corroborated by change-detection observations and show more environmental pressure, agricultural land degradation and an increase of unproductive land-cover classes between 2015 and 2024. signs of change, but also, further, you can see the environmental change process is ongoing. The growing similarity between barren and desert surfaces suggests the formation of degraded transitional zones and further supports findings on desertification trends from change-detection analyses.

Agricultural Land Transformation

The absolute land-cover transformation process detected from 2015 to 2024 was determined as agricultural degradation. The largest change in both datasets was observed in the conversion of agricultural land to barren land, at 45.40% and 30.15% in the VH and VV classifications, respectively (Table 5). Furthermore, agricultural land was transformed to desert sequences by 6.88% and 4.83% in the VH and VV datasets, respectively. The other smaller transitions, from agriculture to built-up areas (2.01–2.75%) and to water bodies (<0.30%), were also considered low [19,22]. The results show a significant loss of agricultural land, and that cultivated areas were the most affected vegetation cover type during the study period. Widespread transformation of cropland into barren and desert land surfaces is presumably linked to prolonged drought, groundwater depletion, soil salinization, low irrigation efficiency, and agricultural abandonment. Moreover, the VH dataset revealed consistently higher transition rates than other datasets, indicating that cross-polarized radar signals are more

sensitive to changes in vegetation structure and biomass. This result indicates that VH polarization is the most sensitive to early stages of agricultural degradation before complete land-cover conversion becomes visually observable. Overall, the identified transitions indicate a declining capacity of land to sustainably support intensive agriculture in the study area as environmental stress increases, within the land's biophysical limits.

All transition percentages reported in this study were calculated from the post-classification transition matrix and represent the proportion of pixels belonging to the source land-cover class that transitioned to the corresponding target class between 2015 and 2024.

Table 5. Major Agricultural Land Transitions Between 2015 and 2024

Transition Type	VH (%)	VV (%)
Agriculture → Barren Land	45.40	30.15
Agriculture → Desert	6.88	4.83
Agriculture → Built-up Area	2.01	2.75
Agriculture → Water	0.28	0.14

Desertification Dynamics

This time series analysis provides significant evidence that desertification persisted throughout the study area during 2015-2024. The conversion of barren land to desert surface, likewise agricultural land, was a significant proportion, Table 6. The most significant transitions to desert are agriculture (6.88% and 4.83% in the VH & VV datasets) and barren land (5.32% and 4.79% in the VH & VV datasets). Detection of relatively smaller contributions by water bodies and the built composition class to the desert surface. These results imply a linear degradation process whereby productive agricultural land is converted into bare surfaces, which are then transformed into desert ecosystems. This sequence is representative of desertification processes following long-term drought, prolonged water scarcity, vegetation loss and unsustainable land use in semi-arid areas. In addition, the over 20% decrease in desert classification accuracy in 2024, observed alongside such high confusion between desert and barren land classes, suggests the development of large transitional zones between classes with very similar physical and spectral properties. Thus, the synergistic information obtained through change-detection and classification-accuracy analyses corroborated the conclusion that desertification has emerged as a significant environmental process affecting landscape dynamics in the study area throughout the research period.

Table 6. Desertification-Related Land-Cover Transitions Between 2015 and 2024

Transition Type	VH (%)	VV (%)
Barren Land → Desert	5.32	4.79
Agriculture → Desert	6.88	4.83
Water → Desert	0.54	0.32
Built-up Area → Desert	0.95	0.76

The transitions that we observe indicate a step-wise degrading pathway:

Land-use Change Dynamics Agriculture→ Degraded Agriculture→ Barren Land→ Desert

This sequence is typical of the desertification processes in semi-arid regions under long-term climatic and anthropogenic stresses. The initial drop in classification accuracy for desert surfaces in 2024 corroborates this interpretation, indicating the development of extensive areas where both barren and desert surfaces are present.

Urban Expansion Dynamics

Another land-use change process that impacted landscape dynamics between 2015 and 2024 was urban expansion. Conversion of agricultural land to built-up areas was 2.01% in the VH dataset and 2.75% in the VV dataset (Table 8), indicating that gradual urban expansion is occurring on previously productive agricultural land. Also, built-up areas showed high persistence, with 11.05% and 11.13% of the study area showing no change between years in the VH and VV data sets, respectively. Urban surfaces are highly stable, characteristic of permanent change and demonstrating that irreversible land use constrains any backward movement once these surface types develop. In 2018, urban sprawl accounted for a smaller share (11.5%) of total land cover transitions than agricultural land degradation and desertification, but it still has considerable environmental consequences because urban growth generally results in the permanent loss of agrarian land and places pressure on physical landscape resources. The urban expansion seen here is likely to indicate not only population growth but also infrastructure development and economic activity within the region. Thus, the interaction between agricultural decline and urban expansion underscores land pressure and reinforces calls for sustainable land-use planning to achieve a balance between future development and environmental conservation.

Table 8. Urban-Related Land-Cover Transitions Between 2015 and 2024

Transition Type	VH (%)	VV (%)
Agriculture → Built-up Area	2.01	2.75
Stable Built-up Area	11.05	11.13

Spatial Distribution of Land-Cover Classes

To visually assess spatial patterns of land-cover distribution, classification maps derived from both polarization modes were analyzed.

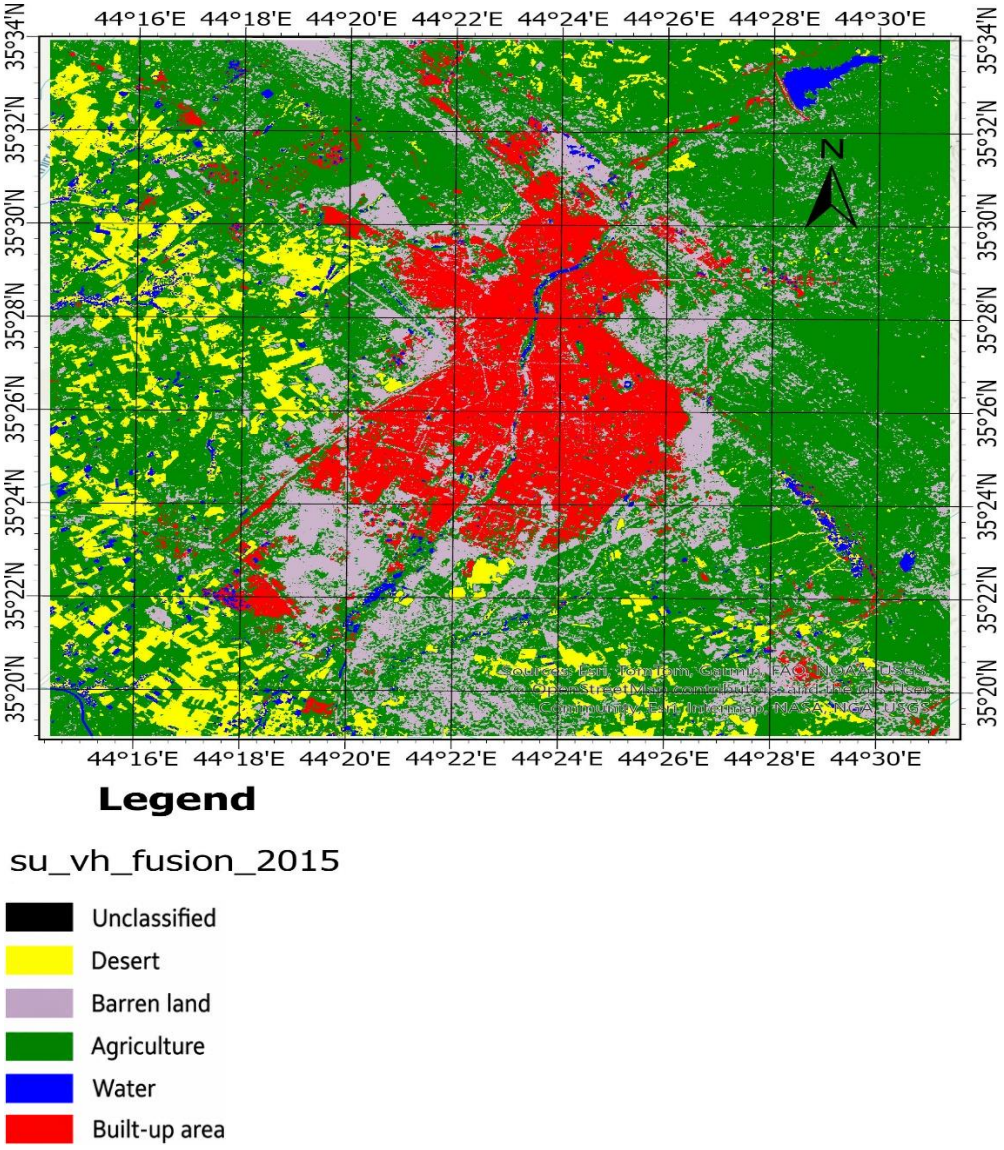


Figure 5. Land-Cover Classification Map Derived from Sentinel-1 VH Fusion (2015).

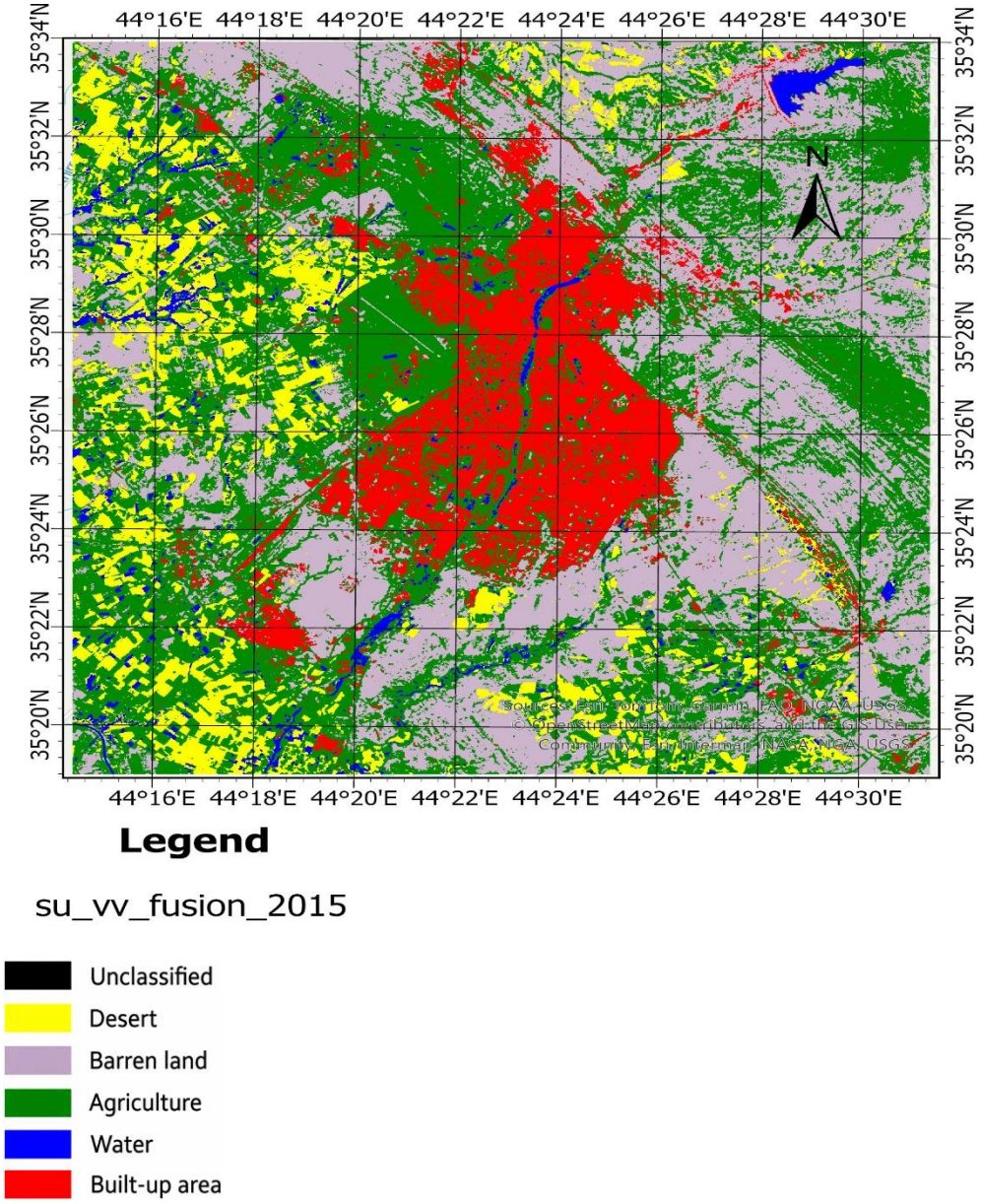


Figure 6. Land-Cover Classification Map Derived from Sentinel-1 VV Fusion (2015).

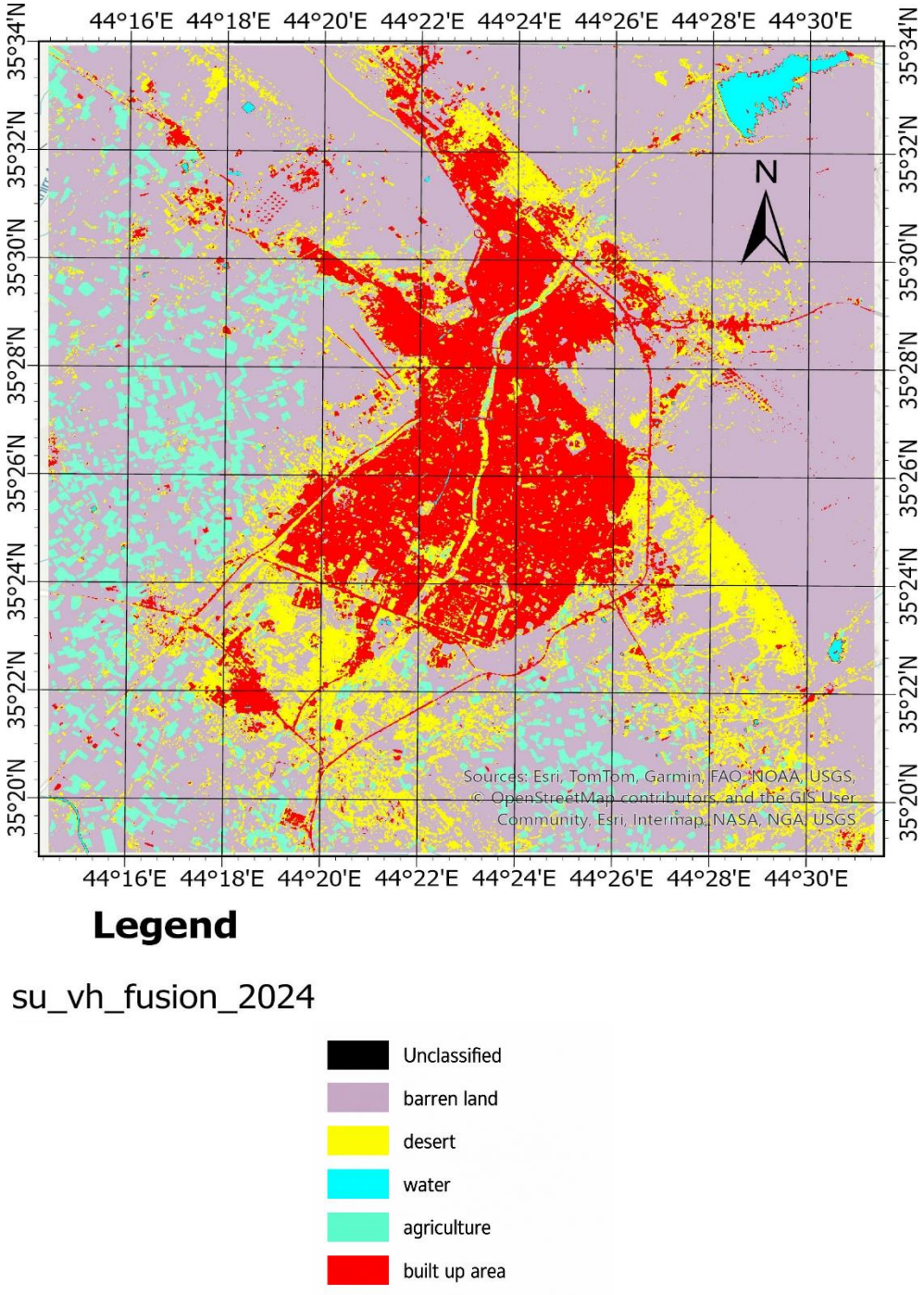


Figure 7. Land-Cover Classification Map Derived from Sentinel-1 VH Fusion (2024).

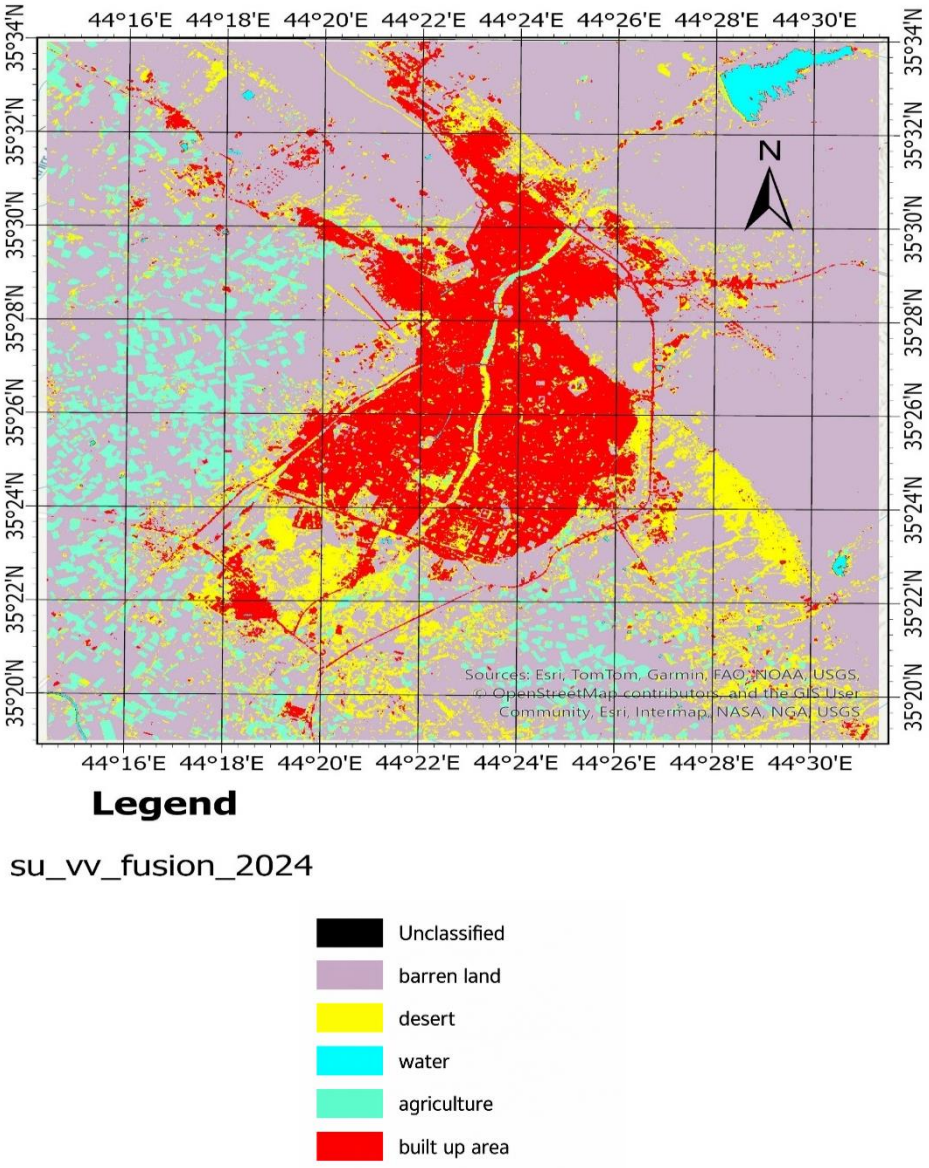


Figure 8. Land-Cover Classification Map Derived from Sentinel-1 VV Fusion (2024).

The land-cover classification maps derived from Sentinel-1 VH and VV fusion datasets reveal substantial spatial changes between 2015 and 2024. In 2015, agricultural land represented the dominant land-cover class surrounding the urban center, particularly in the northern, western, and southeastern parts of the study area. Built-up areas were concentrated within the central urban core, while barren land and desert surfaces were mainly distributed along the peripheral zones. Water bodies were limited and primarily associated with river channels and reservoirs.

By 2024, significant alterations to land-cover distribution had taken shape. Agricultural areas across the globe experienced a significant decrease in area, especially in proximity to barren and desert surfaces. At the same time, barren land is one of the dominant classes in most of the study area, with a declining trend, indicating large-scale land degradation. The desert spread widely around urban areas and agricultural regions, showing the extent of desertification over the past years. The peak of urbanization remained concentrated within the city center, but there was low to moderate sprawl into agricultural lands. Water bodies were relatively more constant, with only slight spatial differences between the two years.

The two classifications (VH and VV) yield similar spatial patterns within their respective areas; however, the VH dataset is more sensitive to vegetation changes and reveals broader areas affected by agricultural expansion. All in all, the classification maps demonstrate unambiguous spatial evidence of agricultural loss, expanding barren and desert surfaces, and continuing urban growth from 2015 to 2024.

Spatial Change Detection Analysis

Spatial change-detection maps provide direct evidence of land-cover transformations during the study period

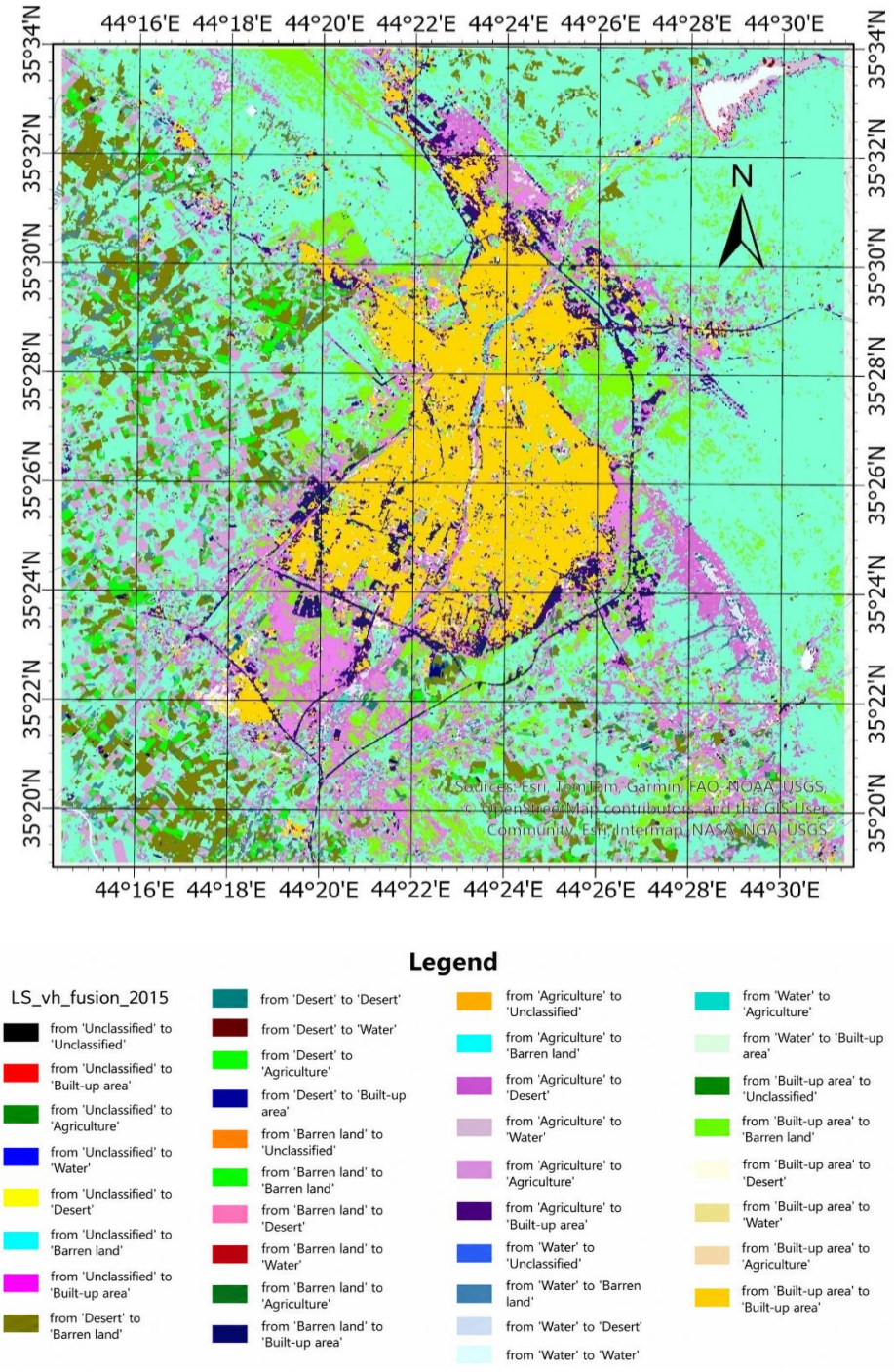


Figure 9. Change Detection Map Derived from Sentinel-1 VH Fusion Data (2015–2024).

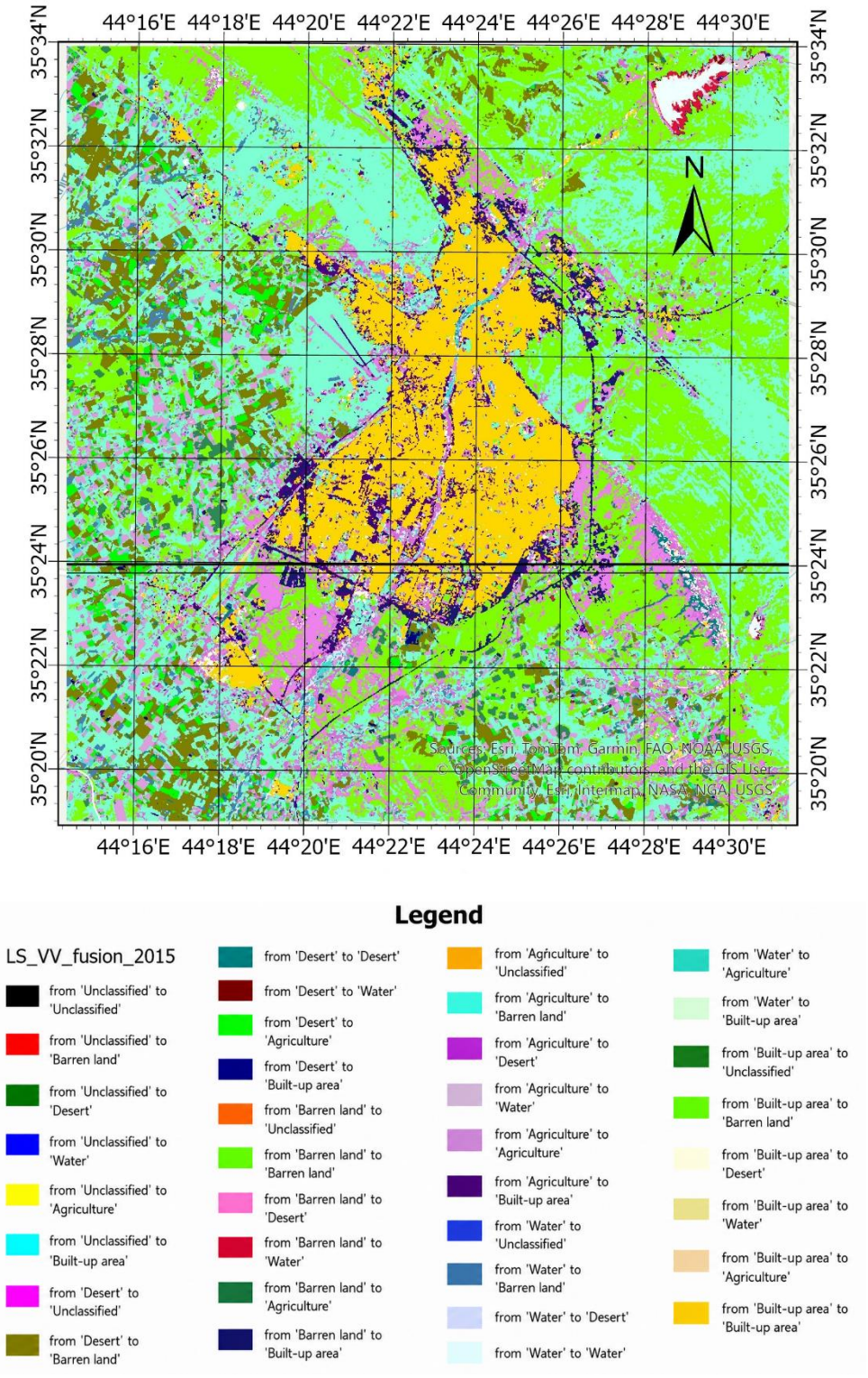


Figure 10. Change Detection Map Derived from Sentinel-1 VV Fusion Data (2015–2024).

The Sentinel-1 VH and VV fusion datasets play an important role in generating change-detection maps showing fine spatial detail of land-cover transitions from 2015 to 2024. The two maps show significant landscape change in the study area, but primarily around agricultural areas and urban fringes/edge of barren land/desert surfaces. The core urban area has undergone relatively little change, but the vast fields and pastures surrounding it have been transformed.

The visual analysis of land change maps shows that most transitions were from agricultural lands to bare ground and desert surfaces in the western, southern, and southeastern regions of the study area. These change–recovery spatial patterns align with the transition matrix results, revealing agricultural degradation as a dominant land-cover-type change process. Additionally, large zones of transition around established barren areas suggest the continued expansion of degraded land and desertification.

The change detection map derived from VH reveals a wider spatial extent of vegetation-related transitions, consistent with the higher sensitivity of cross-polarized radar signals to changes in vegetation structure and biomass. In contrast, the VV change detection map demonstrates greater spatial coherence and a higher proportion of stable classes, indicating better classification accuracy and temporal stability. There is also evidence of localized agricultural-to-built-up transitions at the urban periphery, corroborating moderate levels of urban expansion over the study period.

The change detection maps generally provide strong spatial evidence that agricultural degradation, desertification, and urban growth were the three dominant environmental processes responsible for landscape transformation from 2015 to 2024.

Integrated Environmental Interpretation

The combination of classification accuracy, land-cover transition matrices, classification maps, and change detection results indicates that three main environmental processes have influenced the study area between 2015 and 2024: (i) agricultural degradation; (ii) progressive desertification; and (iii) urban expansion. The consistency among the accuracy assessment, transition statistics, and spatial change maps corroborates these findings, verifying that the detected changes were real rather than a function of classification.

Results reveal that the major environmental trend in the study area is a gradual conversion of agricultural land to barren land and, ultimately, to desert surfaces. The high percentages of transition from agricultural to barren land and from agricultural to desert in both VH and VV datasets support this pathway of degradation. With a rapid decrease in agricultural land and more barren desert surfaces, the expansion indicates increased environmental Pressures from drought, dwindling water availability, & Land deformation.

A secondary transition pathway, in parallel with this, is the conversion of agricultural land to built-up areas, which indicates the impact of urban expansion on the availability of productive land. Urbanization, despite not being as extensive an agent of land degradation and desertification (DG), also entails a permanent change in land use and contributes to the reduction of cultivable space. These processes, in concert, suggest declining agricultural sustainability and stress on natural resources. The complementary contributions of Sentinel-1VH and VV fusion datasets were effective at targeting both stable and dynamic land-cover patterns, providing a consistent and valid basis for long-term environmental monitoring and the sustainable management of natural resources in semi-arid environments.

Conclusions

Sentinel-1 SAR VH and VV fusion datasets were tested in this study for land-use/land-cover (LULC) classification in 2015 and change detection from 2015 to 2024. As indicated by the classification results, the VV fusion dataset achieved the highest accuracy among all datasets since 2015, with an Overall Accuracy of 96.51% and a Kappa coefficient of 0.954, demonstrating excellent classification reliability. Both the VH and VV datasets had lower accuracies in 2024 due to greater landscape complexity and more significant intra-class similarity among land-cover classes, particularly between barren land and desert surfaces.

The substantial environmental changes over the study period were verified through change-detection analysis. The greatest share of agricultural land degradation resulted from land-cover transitions, such as the transformation of vast portions of agricultural land into barren and desert surfaces. The VH dataset can detect more transitions than the VV dataset, indicating that cross-polarized radar signals are more sensitive to vegetation degradation and structural changes. In

addition, substantial conversions from barren land to desert, along with oversaturation of confusion among these classes, are strong indicators that desertification processes were continuing in the study area.

Most areas were urban to a very stable extent during the period studied, and only a moderate amount of agricultural land was lost to urban expansion. Therefore, the maintenance of built-up areas and the conversion of farmland to other urban surfaces constitute well-documented human-induced pressure on productive land resources. Main conclusions: The results identify agricultural degradation, expanding desertification, and emerging urbanization as the predominant environmental processes driving land surface transformations in Mongolia during 2015–2024. The joint application of Sentinel-1 VH and VV fusion datasets represents a robust tool for long-term environmental change monitoring and sustainable land management in semi-arid areas.

References

1. Lillesand, T.; Kiefer, R.W.; Chipman, J. (2015). *Remote sensing and image interpretation*; John Wiley & Sons.
2. Greifeneder, F.; Notarnicola, C.; Hahn, S.; Vreugdenhil, M.; Reimer, C.; Santi, E.; Paloscia, S.; Wagner, W. (2018). The added value of the VH/VV polarization-ratio for global soil moisture estimations from scatterometer data. *IEEE Journal of Selected Topics in Applied Earth Observations and Remote Sensing*, 11, 3668-3679.
3. Reynolds, J.F.; Smith, D.M.S.; Lambin, E.F.; Turner, B.; Mortimore, M.; Batterbury, S.P.; Downing, T.E.; Dowlatabadi, H.; Fernández, R.J.; Herrick, J.E. (2007). Global desertification: building a science for dryland development. *science*, 316, 847-851.
4. Ahmed, Z.; Gui, D.; Abd-Elmabod, S.K.; Murtaza, G.; Ali, S. (2024). An overview of global desertification control efforts: Key challenges and overarching solutions. *Soil Use and Management*, *40*, e13154.
5. Al-Ansari, N. (2021). Water resources of Iraq. *Journal of Earth Sciences and Geotechnical Engineering*, 11, 15-34.
6. Wulder, M.A.; White, J.C.; Loveland, T.R.; Woodcock, C.E.; Belward, A.S.; Cohen, W.B.; Fosnight, E.A.; Shaw, J.; Masek, J.G.; Roy, D.P. (2016). The global Landsat archive: Status, consolidation, and direction. *Remote Sensing of Environment*, 185, 271-283.
7. Moreira, A.; Prats-Iraola, P.; Younis, M.; Krieger, G.; Hajnsek, I.; Papathanassiou, K.P. A. (2013). tutorial on synthetic aperture radar. *IEEE Geoscience and remote sensing magazine*, 1, 6-43.
8. Hameed, M.R.; Fatah, B.A.; Hasan, S.F.; Shareef, M.A. Assessing the Classification of Land Use and Land Cover Using Dual Polarization (VV, VH) Radar Data: An Analysis of the Kirkuk Governorate in Iraq.
9. Torres, R.; Snoeij, P.; Geudtner, D.; Bibby, D.; Davidson, M.; Attema, E.; Potin, P.; Rommen, B.; Floury, N.; Brown, M. (2012). GMES Sentinel-1 mission. *Remote sensing of environment*, 120, 9-24.
10. Veloso, A.; Mermoz, S.; Bouvet, A.; Le Toan, T.; Planells, M.; Dejoux, J.-F.; Ceschia, E. (2017). Understanding the temporal behavior of crops using Sentinel-1 and Sentinel-2-like data for agricultural applications. *Remote sensing of environment*, 199, 415-426.

11. Filipponi, F. (2019). Sentinel-1 GRD preprocessing workflow. In Proceedings of the Proceedings, p. 11.
12. Shakir, B.Q.; Shareef, M.A.; Al Nuaimy, Q.A. (2025). Determination of Soil Properties Utilizing C-Band Synthetic Aperture Radar (SAR) in Southern Kirkuk Governate, Northern Iraq. *Engineering, Technology & Applied Science Research*, 15, 25407-25416.
13. Albanwan, H.; Qin, R.; Tang, Y. (2024). Image fusion in remote sensing: An overview and meta-analysis. *Photogrammetric Engineering & Remote Sensing*, 90, 755-775.
14. Ali, C.A.; Shareef, M.A.S.; Al Nuaimy, Q.A.M. (2024). Estimating Soil Parameters Using C Band Synthetic Aperture Radar in Laylan, Iraq. *Ecological Engineering & Environmental Technology*, 25.
15. Simone, G.; Farina, A.; Morabito, F.C.; Serpico, S.B.; Bruzzone, L. (2002). Image fusion techniques for remote sensing applications. *Information fusion*, 3, 3-15.
16. Fernández-Landa, A.; Johannsen, V.K.; Marchamalo, M.; Fensholt, R. Understanding 'saturation'of radar signals over forests.
17. Joshi, N.; Baumann, M.; Ehammer, A.; Fensholt, R.; Grogan, K.; Hostert, P.; Jepsen, M.R.; Kuemmerle, T.; Meyfroidt, P.; Mitchard, E.T. (2016). A review of the application of optical and radar remote sensing data fusion to land use mapping and monitoring. *Remote Sensing*, 8, 70.
18. Gxokwe, S.; Dube, T.; Mazvimavi, D. (2020). Multispectral remote sensing of wetlands in semi-arid and arid areas: A review on applications, challenges and possible future research directions. *Remote Sensing*, 12, 4190.
19. Mamshai, F.H.A. (2025). Environmental Security and Communal Conflict in Iraq.
20. Shareef, M.A.; Toumi, A.; Khenchaf, A. (2016). Estimating of water quality parameters using SAR and thermal microwave remote sensing data. In Proceedings of the 2016 2nd International Conference on Advanced Technologies for Signal and Image Processing (ATSIP), pp. 586-590.
21. Shareef, M.A.; Hassan, N.D.; Hasan, S.F.; Noori, A.M. (2019). Integrating of GIS and fuzzy multi-criteria method to evaluate land degradation and their impact on the urban growth of Kirkuk city, Iraq. *International Journal of Advanced Science and Technology*, 28, 800-815.
22. Al-Hasani, B.; Abdellatif, M.; Carnacina, I.; Harris, C.; Al-Quraishi, A.M.F.; Maaroof, B.F. (2024). Assessing climate change impacts on rainfall-runoff in Northern Iraq: a case study of Kirkuk Governorate, a Semi-Arid Region. In *Climate Change and Environmental Degradation in the MENA Region*; Springer, pp. 93-111.
23. Azeez, S.M.; Shareef, M.A. (2025). Assessing the Eco-Environmental Quality of Kirkuk City and Taza District Based on Pressure-State-Response Framework for Two Seasons Using Remote Sensing and GIS. *Tikrit Journal of Engineering Sciences*, 32.
24. Sonka, M.; Hlavac, V.; Boyle, R. (1993). Image pre-processing. In *Image processing, analysis and machine vision*; Springer, pp. 56-111.
25. Papadopoulos, S.; Koukiou, G.; Anastassopoulos, V. (2024). Decision Fusion at Pixel Level of Multi-Band Data for Land Cover Classification—A Review. *Journal of Imaging*, 10, 15.

26. Pons, X.; Solé-Sugrañes, L. (1994). A simple radiometric correction model to improve automatic mapping of vegetation from multispectral satellite data. *Remote sensing of Environment*, 48, 191-204.
27. Tian, Y.; Shi, Y.; Liu, X. (2012). Recent advances on support vector machines research. *Technological and economic development of Economy*, 18, 5-33.
28. Zhang, C.; Tian, Y.; Deng, N. (2010). The new interpretation of support vector machines on statistical learning theory. *Science in China Series A: Mathematics*, 53, 151-164.
29. Suykens, J.A. (2001). Nonlinear modelling and support vector machines. In Proceedings of the IMTC 2001. proceedings of the 18th IEEE instrumentation and measurement technology conference. Rediscovering measurement in the age of informatics (Cat. No. 01CH 37188), pp. 287-294.
30. Bernard Tso, P.M.M. (2009). *classification methods for remote sensing data* CRC,Taylor and Francis Group.
31. Chen, J.; Gong, P.; He, C.; Pu, R.; Shi, P. (2003). Land-use/land-cover change detection using improved change-vector analysis. *Photogrammetric Engineering & Remote Sensing*, 69, 369-379.
32. Abd El-Kawy, O.; Rød, J.K.; Ismail, H.; Suliman, A.S. (2011). Land use and land cover change detection in the western Nile delta of Egypt using remote sensing data. *Applied geography*, 31, 483-494.
33. EX, E. ENVI EX user's guide. 2009.
34. Jensen, J. R. (2015). *Introductory Digital Image Processing: A Remote Sensing Perspective*. Pearson Education. https://books.google.de/books?id=BWx3CgAAQBAJ